Summer 2020

Influence of input energy on mechanical properties of laser powder bed fused AISI 304L stainless steel

Tan Pan

Department:

INFLUENCE OF INPUT ENERGY ON MECHANICAL PROPERTIES OF LASER POWDER BED FUSED AISI 304L STAINLESS STEEL

by

TAN PAN

A THESIS

Presented to the Graduate Faculty of the

MISSOURI UNIVERSITY OF SCIENCE AND TECHNOLOGY

In Partial Fulfillment of the Requirements for the Degree

MASTER OF SCIENCE

in

MANUFACTURING ENGINEERING

2020

Approved by:

Dr.Frank Liou, Advisor
Dr.K. Chandrashekhara
Dr. Lianyi Chen

PUBLICATION THESIS OPTION

This thesis consists of the following one article, formatted in the style used by the Missouri University of Science and Technology:

Paper I, found on pages 5–38, is intended for submission to *Additive Manufacturing Journal*.

ABSTRACT

Powder Bed Fusion process with selective laser melting technique is popularly adopted in additive manufacturing area on account of its layer by layer manufacturing fashion capable of fabricating components with complex internal and external geometries and structures. However, the process-property map is unique and vital for different materials and AM configurations used for fabrication. The process parameter is identified as a significant factor that heavily influences the properties and performances of the printed materials.

Current work aimed to extend the existing knowledge on Laser Powder Bed Fusion fabricated AISI 304L by accessing the influence of varying energy input on the mechanical performance. 304L specimens with densities ranging from ~97% to ~99% were produced by varying scan speed and hatch spacing. The result indicated no distinguishing difference was observed of density, hardness, ultimate tensile strength, and uniform elongation once energy density reached more than $47.6\,\mathrm{J}/mm^3$. Below this ED, lack of fusion and insufficient overlaps between adjacent scan tracks gave rise to the poor bonding in and between layers, which induced the poor mechanical performance of the printed metal. However, at the highest energy density, impact toughness was also deteriorated by the keyhole porosity induced by the excess remelting and accumulated along the partition line. Anisotropy in tensile and impact performance was clearly observed. By means of varying input energy put the anisotropy in impact performance was modified.

ACKNOWLEDGMENTS

Foremost, I would like to express my sincere gratitude to my primary supervisor, Dr. Frank Liou, for his expertise, patience, support, and guidance throughout my graduate education. His unwavering enthusiasm for researching keeps me engaged with my study and work to complete the thesis successfully.

Additionally, I wish to show my deep appreciation to the rest of my committee members, Dr. K. Chandrashekhara and Dr. Lianyi Chen, for their valuable assistance and insightful comments during the process of my research.

I would like to thank the colleagues in my laboratory group for their help and teamwork and express distinct appreciations to Dr. Sreekar Karnati, Dr. Xinchang Zhang, Dr. Yunlu Zhang, Wenyuan Cui, Lan Li, Dr. Lei Yan, Yitao Chen, Todd Spark, Aaron Flood, and Mohammad Masud Parvez.

I wish to extend special thanks to my family for their selfless love and financial support, and my friends for their supportive encouragement and moral support.

I also place on record, my sense of gratitude to one and all who, directly or indirectly, gave their kind hand in this research venture.

TABLE OF CONTENTS

LIST OF ILLUSTRATIONS

PAPER I Page

LIST OF TABLES

NOMENCLATURE

Symbol	Description
P	Laser Power
v	Scan Speed
h	Hatch Spacing
t	Layer Thickness

1. INTRODUCTION

Powder bed fusion (PBF) based technology is a popular class of techniques in Additive Manufacturing (AM) that consolidates powder layers into components. In general, the powder bed fusion process consists of an energy source e.g., laser or electron beam, a powder bed, a build chamber, a coating system, and a gas-circulating system. The energy source is utilized to selectively scan and melt each layer after spreading with uniform powder. The scan pattern at each layer is controlled by the input digital STL file. After the completion of one layer, the building substrate drops down at a defined layer thickness and the powder chamber goes upward by the same layer thickness or drops a dose of powder depending on the location of the powder hopper. A roller or wiper then uniformly spread and pack the powder across the build chamber to continue the scanning at the current layer. The whole cycle is repeated layer by layer until the completion of the build processing [1]. Among the PBF methods is the selective laser melting (SLM) process which utilizes a laser beam to melt particles to facilitate the creation of light-weight, small-sized parts. Its layer by layer manufacturing nature also realizes the capability to manufacture components with complex external and internal geometries and structures, which is different to achieve with conventional manufacturing method. However, SLM still suffers from the presence of porosity inside the built parts which could impact the microstructure and mechanical performance of the fabricated specimens to some extent. Previous researches have studied the effect of densification for different material including stainless steel 316L [2–7], Aluminum alloy [8], 17-4PH stainless steel [9,10], and Ti6Al4V [11]. It is well known that the densification of the fabricated part can be significantly

influenced by the involved process parameters. An equation to representing the energy density can be applied here to capture the effects of laser power, layer thickness, travel speed, and hatch spacing as Equation 1.

$$ED = \frac{P}{v \times h \times t} \tag{1}$$

where P is the laser power, v is travel speed of the laser, h is hatch spacing and t is layer thickness.

Stainless steel 316L and 304L are well known as the materials with notable corrosion resistance, oxidation resistance, and low cost. Researchers focused on the optimization of the process parameters to maximize the densification of the printed parts as well as achieve better mechanical behaviors with the powder bed fusion system. Tucho et al. investigated the effect of process parameters on the densification, microstructure, and hardness properties for stainless steel 316L fabricated with the SLM process. Within the range of ED between 50 and 80J/mm^3, the porosity decreased exponentially and varied from ~ 3.4% to ~ 0.2 %. Hardness increased linearly with increasing energy density [12]. Cherry et al. controlled the point distance and exposure time to vary the ED from 41.81 to 209.03J/mm^3. The minimum amount of porosity (~0.38%) was observed at 104.52J/mm^3 with hardness decreased with increasing porosity [13].

Some researchers also worked on the tensile properties of SLM fabricated parts with variations in process parameters. Wang et al. [14] concluded that the crystal morphology and grain size were significantly influenced by the variation in energy input. A Vicker hardness of 281.6 HV, 590 MPa in tensile strength and 21.1% in elongation were provided by the optimal ED at 125 J/mm^3. Guan et al. [15] figured out the minor influence

of slice thickness and overlap rate. Also, they indicated the hatch angle of 105 degrees could provide better tensile properties.

Due to the layer by layer fashion of AM, the uniformity and consistency of mechanical performances of the printed metal are also vastly influenced by anisotropy. Guan et al. [15] and Shifeng et al. [16] observed the specimens printed in vertical orientation behaved the best tensile properties in comparison to the horizontal direction. However, many researchers gained the opposite results. In Liverani et al.'s work [17], they observed that with ED in a range between 102 and 214.3J/mm^3inducing the resultant densities > 98%, strength increased when the build orientation changed from 90 degree to 45 degree. Increases of ~10–20% in yield strength and 12–13% in ultimate tensile strength were recorded at $\alpha = 45°$ compared to $\alpha = 90°$ while the elongation of samples built at 45° decreased by about 50% in comparison to those built at 90°. Casati et al. [18] observed that the tensile strength and ductility of specimens built in horizontal orientation were better and explained that the layer boundary with possibly high concentration of defects could be the reason for the low strength in vertical orientation.

The part density and mechanical properties including tensile property in different orientations and (micro)-hardness varying with energy density were summarized in Table 1.1 for reference.

Table 1.1. The summary table for the density and mechanical properties variation with energy density.

Paper	Energy density (J/ mm^3)	Part density	Strength (MPa) w.r.t orientation		Elongation (%)	Hardness
			YS	UTS		
Tucho [12]	50-80	96.57% - 99.86%				185±9, 213±3 HV
Liverani [17]	102-214.3	98.4% - >99.9 %	45°: 510-540; 90°: 430-495	45°:615-650; 90°: 550-580	25-70	
Suryawanshi [19]	20		SM0° 511.6±14	621.7±12	20.4±3	
			SM90° 430.4±11	509±3	12.4±1	
			CB0° 536.4±4	668.4±5	24.7±2	
			CB90° 448.5±20	527.9±7	11.6±1	
Casati [18]	48.48		0°: 554±4.6	684.7±4.7	36.3±2.1	
			90°: no YS	580.7±14.5	25.7±12.2	
Cherry [13]	41.81-209.03	91% - 99.62%				162-225 HV10
Nguyen [20]	37-110	91.2% - 99.9%	~ 485±15	~ 712±12	~ 61%	
Wang [14]	104.17-178.57	94.4% - >98%		525-675	14-21.5	252-281.6 HV0.1
Ahmadi [21]	51.19-90		265-524	280-647	0.68-15.74	
Shifeng [16]	167			506-726	9.2-63.5	

PAPER

I. INFLUENCE OF INPUT ENERGY ON MECHANICAL PROPERTIES OF LASER POWDER BED FUSED AISI 304L STAINLESS STEEL

ABSTRACT

In additive manufacturing (AM), the process-property map is unique and vital for every material and may vary with the AM modality used for fabrication. The properties and performance of the material can be heavily impacted by varying process parameters. The aim of the current study was to extend the existing knowledge on Laser Powder Bed Fusion fabricated AISI 304L by evaluating the influence of varying energy input on mechanical performance. In this work, 304L specimens with densities ranging from ~97% to ~99% were produced by varying scan speed and hatch spacing. For this AM implementation, a minimum of 47.6 J/mm^3 was found to be necessary for attaining greater than 99% relative density. While no distinguishable differences were found in hardness values, the tensile and impact performance was found to be significantly different with varying energy density. Also, anisotropy in tensile and impact performance was clearly observed. Anisotropy in strength was found to vary with input energy density. However, no discernable trends were observed. At low relative densities, the elongation in the vertical direction was observed to be lower than the horizontal direction. However, at densities greater than 99%, the vertical elongation values were larger than the horizontal. The input energy density also affected the failure mechanism during impact testing. Distinct features indicating crack propagation along the inter-track boundary, clusters of key hole porosity

and lack of fusion defects were found on fracture surfaces. By means of varying input energy, the anisotropy in impact performance was modified and improved.

Keywords: powder bed fusion; 304L stainless steel; tensile testing; Charpy testing; anisotropy

1. INTRODUCTION

Laser Powder Bed Fusion (LPBF) is one of the major additive manufacturing technologies that is seeing aggressive incorporation into various streams of the manufacturing industry. With increasing maturity, the ease of LBPF incorporation and financial viability has also been increasing [1]. However, the vast potential of this technology is yet to be fully realized. One of the bottleneck issues stunting the incorporation of this technology is the limited list of fully viable materials. Developing viable process parameters for a new candidate material can be a long and challenging task.

The LPBF process has a very complex implementation and involves the setup and use of a long list of process parameters [2]. Depending on the material and geometry under consideration, the emphasis and attention paid to these parameters can be significantly different. Therefore, the development process for a fully viable process parameter setup requires multiple stages of the investigation. The first stage of this setup process is always the identification and optimization of parameters necessary for producing near 100% dense material. During this stage of development, the process parameters are adjusted to account for issues such as balling [3], porosity [4], residual stress [5], etc. Depending on the type

of the material, implementation of the LPBF process, and the machine architecture, the types, and values of these parameters can be significantly different.

In most LPBF platforms, the parameters that can affect the densification of material are primarily laser power, scan speed, hatch spacing, layer thickness, and scan strategy. To capture the combined effect of these parameters, energy density, as defined in Equation (1), is popularly used [6–8].

$$\mathrm{ED} = \frac{P}{v \cdot t \cdot h} \tag{1}$$

where P is the laser power, v is scan speed, h is hatch spacing and t is the layer thickness.

In a densification study, the values of energy density are varied through its constituent parameters to increase the density of the fabricated material. Getting full density in a build can be impeded by the formation of porosity. Researchers have performed several studies to characterize the mechanism of pore formation in LPBF. This was achieved through the comprehensive analysis of material produced through systematic manipulation of process parameters. In these studies, multiple methods of porosity quantification were employed. Methods such as density testing [8–13], optical microscopy/metallographic analysis [8–16], and X-ray CT [11,13,15–17] were found to be most effective in density quantification. Manipulation of process parameters to achieve dense material was shown to be feasible for materials such as stainless steels [8–12,17–19], aluminum alloys [15], and titanium alloys [13]. However, most of these studies were concluded with the identification of one or a couple of viable setups and seldom extended into further exploration of viable process domain. While details of porosity are comprehensively discussed, the scope of these investigations into exploring mechanical properties and their dependence on process parameters is still very limited.

Stainless steel 304 is favored in many streams of industries due to its superior corrosion resistance, excellent mechanical behavior, and low cost. This material is especially of great value to the nuclear industry [20–23]. Incorporation of this material into LPBF systems, therefore, carries great value. Currently, limited literature exists on the study and use of 304 stainless in the LBPF process. Especially on the aspect of varying energy density. Nguyen et al. [24] studied the mechanical properties of 304L stainless steel fabricated by LPBF using energy densities between 37 to 110 J/mm^3. Their established optimal process parameter provided the highest relative density of 99.99%. They reported that an increase in strength resulted from the presence of the nano-cellular structure, martensite phase, fine grains, and nano-size carbides. Also, the presence of a negative (compressive) residual stress was attributed to the increase in strength.

AISI 316L, a close relative to AISI 304 stainless steel, is popularly used in the LBPF process. The main difference in chemical composition demonstrates that 304L contains 18.0-20.0 Cr and 8.0-12.0 Ni while 316L is comprised of 16.0-18.0 Cr, 10.0-14.0 Ni, and 2.0-3.0 Mo. The addition of Mo in 316L provides improved strength and corrosion resistance [25]. AISI 316L is of great interest to the aerospace industry and has therefore been one of the first materials to be incorporated into the LPBF process. Due to the similarity in thermal, physical, and chemical properties between the two materials, the authors believe understanding influence on varying energy density on 316 is relevant to understanding 304L behavior. Tucho et al. [26] studied the effect of process parameter variation on the resulting porosity, microstructure, and hardness properties of 316L fabricated with the SLM process. Between energy density values of 50 to 80 J/mm^3, they found that with increasing energy input, the porosity decreased exponentially. In this range

of energy density, the porosity dropped from 3.4% to around 0.2%. Also, hardness was seen to increase linearly with increasing energy density. Similarly, Cherry et al. [27] looked into the effect of energy density on the LPBF processing of 316L with regards to porosity, surface finish, microstructure, density, and hardness. They varied the energy density by varying the point distance and exposure time and manipulated energy density between 41.81 to 209.03 J/mm^3. They noticed that the least amount of porosity was observed at 104.52 $J/mm^3$with a relative density of 99.62%. It was also noticed that the hardness values decreased with increasing porosity. Depending on the machine, power range, spot size, etc. different values of energy density were observed to produce similar densification in SS 316L. Therefore, a common baseline for minimum energy density might not be viable for different machine setups and architectures. However, a baseline energy density for similar make and architecture might still be a possibility.

Along with the influence of energy density on densification, the anisotropy in tensile properties with build orientation was also reported in the literature. Specific to 304, Guan et al. [28] studied the variation in tensile properties of SLM parts with different build orientations and indicated the best tensile properties were achieved with the gage section perpendicular to the build orientation. Also, many other researchers [29–32] demonstrated that tensile properties varied with build orientations for stainless steel 316. While anisotropy was reported, its dependence on input energy density has not been well documented.

To fill the existing knowledge gap on mechanical properties of LPBF produced AISI 304L, the authors in this investigation aim to evaluate the influence of varying energy density on mechanical properties and anisotropy in stainless steel 304L. By systematically

changing the input energy, the authors hope to achieve near dense material at multiple sets of process conditions. By doing so, the authors aim to quantify the bounds of mechanical performance of LPBF produced 304L stainless steel.

2. MATERIALS AND METHODOLOGY

2.1. EXPERIMENTAL PROCEDURE AND PROCESS PARAMETERS

The AM material studied in the current investigation was fabricated using the Renishaw AM 250 located at Missouri University of Science and Technology. Figure 1 shows the inner chamber of the AM 250 with annotations to the different critical components. The AM 250 is equipped with an Nd-YAG pulsed laser capable of producing a peak power of 200W beam with a Gaussian intensity profile. During the deposition, the substrate and powder in the chamber were maintained at 80°C to reduce the influence of water content in the powder. During the build, the oxygen level inside the build chamber was maintained to be below 1000 ppm. A constant volumetric recirculating gas flow of 400 ft/mm^3 argon gas was maintained to remove ejecta and condensate generated during deposition.

The Renishaw AM250 employs a spot-by-spot melt method as opposed to the more popular continuous melting process. Along the defined tool path, the laser is scanned in discrete steps where the beam is held stationary to meet a certain time of exposure and then moved to the next point by a predefined distance. A schematic illustration detailing the process is shown in Figure 2. The general tool path strategy used here is referred to as stripes, where the region to be scanned is divided into bands of pre-defined width. The laser

is scanned along the width of these bands. Between successive scans, a certain amount of overlap is maintained to achieve densification, this is referred to as hatch spacing. Also, a certain amount of overlap is to be present between the bands to achieve densification between bands. The first stage of process optimization would, therefore, involve the identification of optimal values for these parameters.

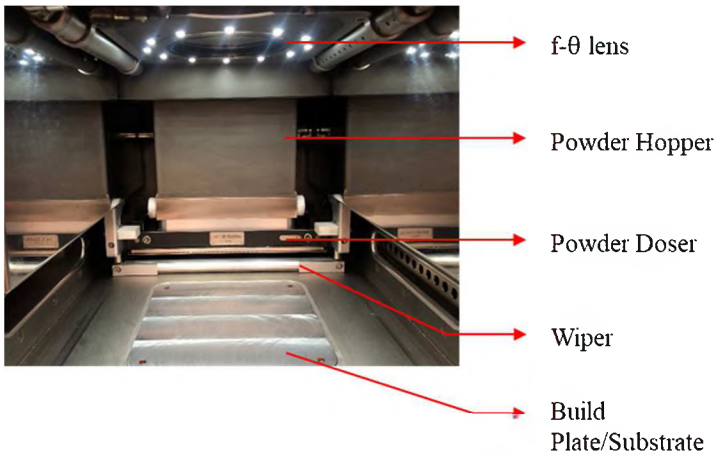

Figure 1. The inner chamber of Renishaw AM250 powder bed machine.

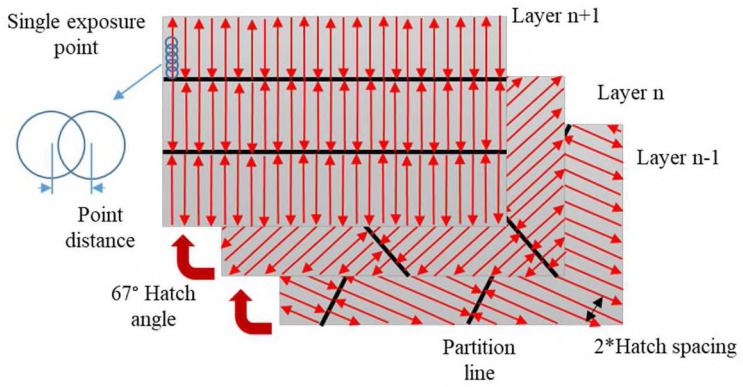

Figure 2. The diagram to explain some of process parameters.

Prior to this study, the AISI 304L nominal parameters used on this machine were based on previous work by Ben Brown [33]. The optimization process involved the identification of optimal parameters that produced a flaw-free bead on the plate. That initial optimization was followed by successful scaling of these process parameters to achieve near dense bulk material. His optimization of parameters resulted in specimens with greater than 99% relative density. The values of the optimal parameters are listed below.

Table 1. The detailed values of the nominal parameter.

Laser power (W)	Point distance (µm)	Exposure time (µs)	Hatch spacing (µm)	Layer thickness (µm)
200	70	88	85	50

Table 2 summarizes the tensile properties of the AISI 304L fabricated with the above-mentioned nominal parameters. This table is a compilation of previous works as well as characterization performed for the setup of this study [34,35]. The tensile testing was performed using miniature specimens, specifics of this testing are discussed in the later sections. The impact testing was performed on as-built Charpy bars with machined V-notch, details of testing are discussed below. From the properties tabulated in Table 2, the anisotropy in the as-built material is apparent. The tensile strength in the horizontal direction (gage section perpendicular to building direction) was observed to be better than the strength in the vertical direction (gage section along build direction). Similarly, the impact toughness was observed to be the lowest and most variant in the vertically built specimens and highest in the horizontally built specimens.

Table 2. Tensile strength and impact toughness (as built condition) of SLM printed 304L with nominal parameter from [34,35].

	YS (0.2% offset) (MPa)		UTS (MPa)		Impact toughness (J)	
	Mean	Std Dev	Mean	Std Dev	Mean	Std Dev
Horizontal	494.7	11.9	670.4	20.6	166.5	21.8
45 Inclined	514.2	12.0	699.0	9.1	167.3	19.2
Vertical	467.8	24.2	614.3	35.0	123.9	45.3
Wrought					210.0	15.0

In the current effort, the process parameters were varied with the intention of varying input energy while still attaining near dense material. To do so, the point distance and hatch spacing were identified as key variables. A total of three levels for point distance and five levels of hatch spacing, yielding a 2-way full factorial experiment of 15 parameter sets was setup. The exposure time was held constant at 88 μs. Similarly, layer thickness at 50 μm and laser power at 200W were held constant. To enable the calculation of energy density as defined in equation 1, scan speed v was defined as shown in Equation (2).

$$v = \frac{Point\ distance}{Exposutre\ time} \tag{2}$$

The details of the parameter combination are tabulated in Table 3. The energy density was determined based on Equation 1. The nominal parameter was coincident with the parameter set number 8 in Table 3.

Table 3. The process parameter of Renishaw AM 250 for fabrication 304L stainless steel.

Energy density number (ED #)	Laser power (W)	Point distance (µm)	Exposure time (µs)	Scan speed (m/s)	Hatch spacing (µm)	Layer thickness (µm)	Energy density (J/mm^3)
1	200	53	88	0.6	65	50	102.6
2	200	53	88	0.6	75	50	88.9
3	200	53	88	0.6	85	50	78.4
4	200	53	88	0.6	95	50	70.2
5	200	53	88	0.6	105	50	63.5
6	200	70	88	0.8	65	50	76.9
7	200	70	88	0.8	75	50	66.7
8	200	70	88	0.8	85	50	58.8
9	200	70	88	0.8	95	50	52.6
10	200	70	88	0.8	105	50	47.6
11	200	88	88	1.0	65	50	61.5
12	200	88	88	1.0	75	50	53.3
13	200	88	88	1.0	85	50	47.1
14	200	88	88	1.0	95	50	42.1
15	200	88	88	1.0	105	50	38.1

2.2. MATERIAL

The material used in this study was Argon gas-atomized stainless steel 304L procured from LPW Technology. The chemical composition of this powder is tabulated in Table 4. An image of the powder particles captured on a Hitachi 4700 scanning electron microscope (SEM) shows the nearly spherical morphology of the 304L stainless steel powder particles (Figure 3).

Table 4. The chemical composition of stainless steel 304L powder particles and wrought stainless steel 304L bar stock in weight percentage.

Element	C	Cr	Cu	Fe	Mn	N	Ni	O	P	S	Si
Powder	0.018	18.4	<0.1	bal	1.4	0.06	9.8	0.02	0.012	0.005	0.6
Wrought	0.03	18-20	-	bal	2	0.01	8-12	-	0.045	0.03	1

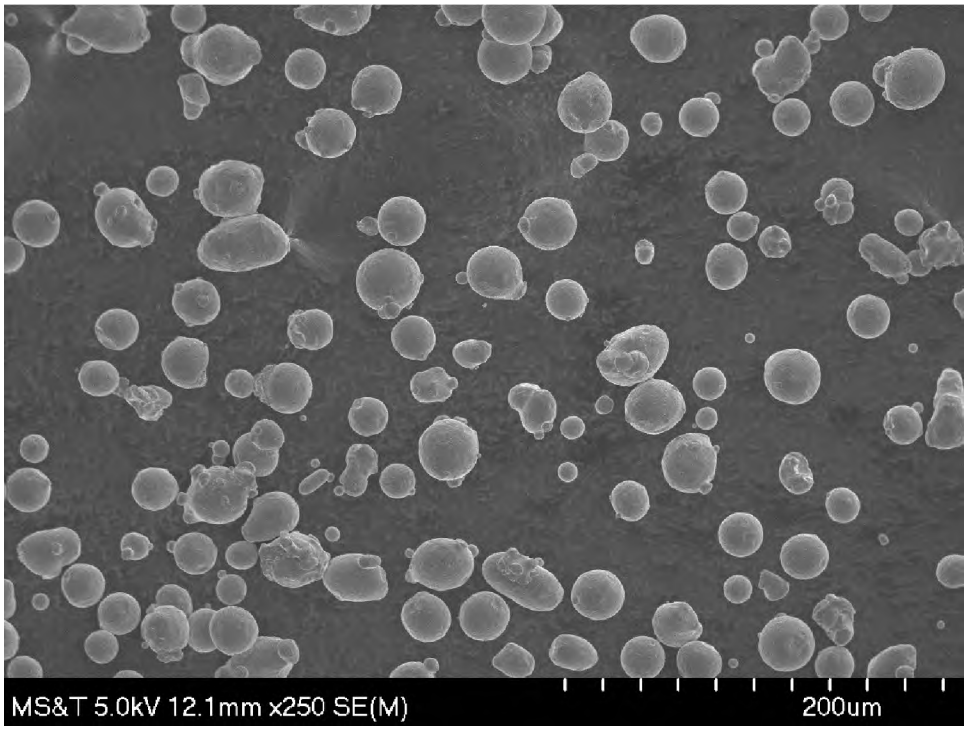

Figure 3. A sample of the morphology of stainless steel 304L powder particles.

2.3. MATERIAL CHARACTERIZATION

The first build (Build I) was fabricated with the above 15 parameter sets for density testing and tensile testing. The specimen design dimensions were 12 mm (in x-direction) * 12 mm (in y-direction) *15 mm (in z-direction/ build direction). Three replicates were fabricated for each parameter set. The second build (Build II) was manufactured for impact

toughness testing. The design dimension of the specimens was 10 mm (in x-direction) * 10 mm (in y-direction) *57 mm (in z-direction/ build direction). Five replicates were made for each parameter set. The locations of all these specimens of different parameter sets were completely randomized on the build plate. All specimens were cut from the substrate on a Sodick VZ300L Wire EDM.

2.3.1. Density Testing and Microstructure Examination. Density testing was based on the Archimedes principle and was performed for Build I specimens in as-built condition. Later, sections of these cuboids were cut along the x-y plane to prepare specimens for metallography. These sections were mounted in epoxy, ground with abrasive papers (400, 600, 800, and 1200 grit) and polished with silica suspension (9, 3, 1, and 0.05 μm). Electro-etching was performed in 40 ml deionized water and 60 ml HNO3 mixture at a voltage of 5V for 5s. The microstructure of the specimens was examined and imaged under an optical microscope (OM, Hirox KH-8700 Microscope).

2.3.2. Hardness Testing. Micro-hardness and hardness testing were performed on these sections using a Duramin hardness testing machine (Struers, Cleveland, OH, USA). A Vickers diamond indenter was used to apply a load of 1.96 N for 5s and 9.81N for 10s duration for microhardness and hardness values.

2.3.3. Tensile Testing. From the remaining Build I specimen materials, miniature dog bone specimens [34] were cut to perform tensile testing for each parameter set. These miniature tensile specimens were in two orientations. One with the gage length parallels to the build direction (vertical) and the other perpendicular (horizontal) to the build direction. The dimensions of the miniature tensile specimen are shown in Figure 4. These specimens have a nominal thickness of 1 mm. These specimens were cut to shape using the Sodick

wire EDM. The process was optimized to obtain a minimal recast layer. Also, prior to performing the testing, these miniature tensile specimens were polished with 800 grit SiC paper. The tensile testing was performed on an Instron UTM machine. As per the ASTM E-8 standard, the test involved 2 stages. First, the test was strain-controlled using extensometer feedback to achieve a strain rate of 0.015mm/mm/min. After a strain of 1%, the extensometer was removed and was then controlled by the constant crosshead speed of 1.5mm/min. More than 6 specimens were tested per each process parameter and cut orientation. After the tensile testing, the fracture surfaces of the broken miniature tensile specimens were examined on an SEM (FEI Helios Nanolab 600).

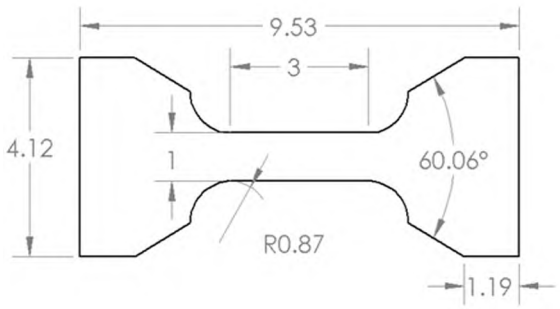

Figure 4. The dimension of mini-tensile specimens. All dimensions are in mm.

2.3.4. Charpy Testing. Charpy specimens from Build II were extracted from the build plate and tested according to ASTM Standard E23. However, the specimens were tested in the as-built surface condition. A "V" notch of 2 mm depth was machined using a standard broach. The depth of the notch was validated through optical microscopy. A minimum of 6 samples was tested for each parameter set. After the Charpy testing, the fracture surfaces of the broken Charpy specimens were examined on an Aspex 1020 SEM.

2.4. BUILD WITH PROCESS PARAMETER OPTIMIZED FOR IMPACT TOUGHNESS

After analyzing the impact toughness of the specimens built in Build II, the parameter set that yielded the highest median toughness values was obtained. Build III was fabricated with Charpy specimens of this parameter set. Specimens in three build orientations, horizontal (0), inclined (45), and vertical (90) were fabricated to study the anisotropy in impact toughness. The specimen layout of Build III is shown in Figure 5. The number of the tested specimens in each build orientation is listed in Table 5. Density testing, microstructure evaluation, Charpy testing, fractography, and tensile testing were again performed on Build III specimens.

Figure 5. The layout for Build III with toughness optimized parameter in three build orientations.

Table 5. The number of Charpy specimens in each orientation fabricated in Build III.

Material	Orientation	Number of Specimens
SLM, As-built	0	22
	45	20
	90	25

3. RESULTS AND DISCUSSIONS

3.1. DENSITY AND POROSITY

The measurements of bulk density and calculated porosity vs. energy density are shown as plots in Figure 6. These density measurements were performed on the Build I cuboid samples. It can be observed that the median density value of the fabricated material gradually increased up to an energy density of 58.8 J/mm^3 and then stabilized. Using the bulk density values, relative density values were calculated against the density of the powder. The porosity values were then calculated by subtracting the relative density values from 1. The porosity values were observed to be less than 1% for energy density values greater than 47.6J/mm^3. However, the highest porosity produced was ~ 3% for the lowest energy density values at 42.1J/mm^3. These differences in density were ascertained to be statistically significant through a one-way ANOVA analysis. The absence of porosity with increasing energy density implies, sufficient overlap between successive laser scans and consecutive layers were successfully achieved. From the density values, more than 99% density was achieved for ED greater than 47.6J/mm^3. This implies, for ED higher than the 47.6 J/mm^3threshold, excess energy is being used for producing >99% dense material. In the current process domain, slower scan speeds and closer hatch spacing are the means to

achieving higher energy density. Higher energy densities are therefore slower rates of fabrication. If density was the only sufficient criteria, using higher energy densities can mean lower productivity.

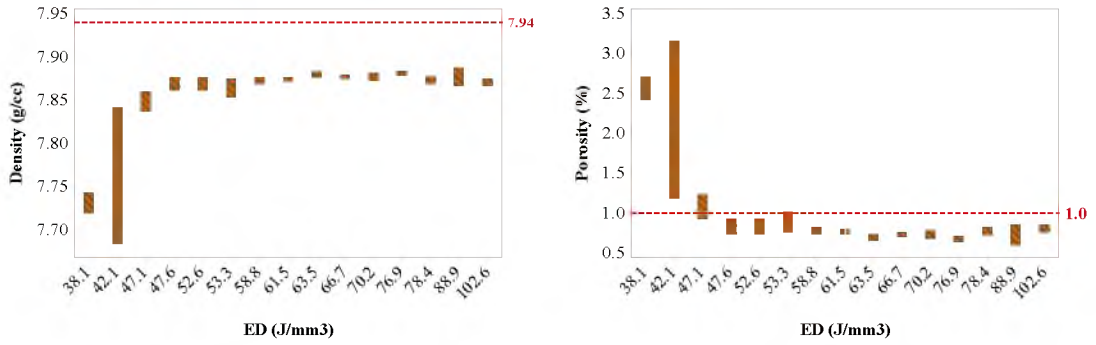

Figure 6. The density and porosity data with varying energy density.

3.2. MICROSTRUCTURES

At lower energy densities, relatively larger scan speeds and wider hatch spacing are expected to produce a lack of sufficient fusion between successive scans and layers. To validate this hypothesis, x-y (in layer) cross-sections were analyzed under OM. The images of specimens built with the lowest, median, and highest ED were shown in Figure 7. At the lowest ED (Figure 7 (a)), irregular shaped pores and streaks of such pores were observed throughout the cross-section. The shape and the pattern in porosity suggest a lack of fusion and/or insufficient overlap as a likely source for porosity formation. The streak pattern of porosity and its occurrence in the x-y section suggests porosity could be located between adjacent laser scans. At the median ED value (Figure 7 (b)), the nominal ED, porosity was observed to be insignificant and rarely found. However, at the highest energy density values (Figure 7 (c)), lines of circular pores were observed in highly localized regions. The

circular shape of these pores suggests, gas porosity could be the likely origin. The localization of this porosity was hypothesized to be an outcome of the tool path. Apart from these clusters of pores, no other variant of porosity was observed.

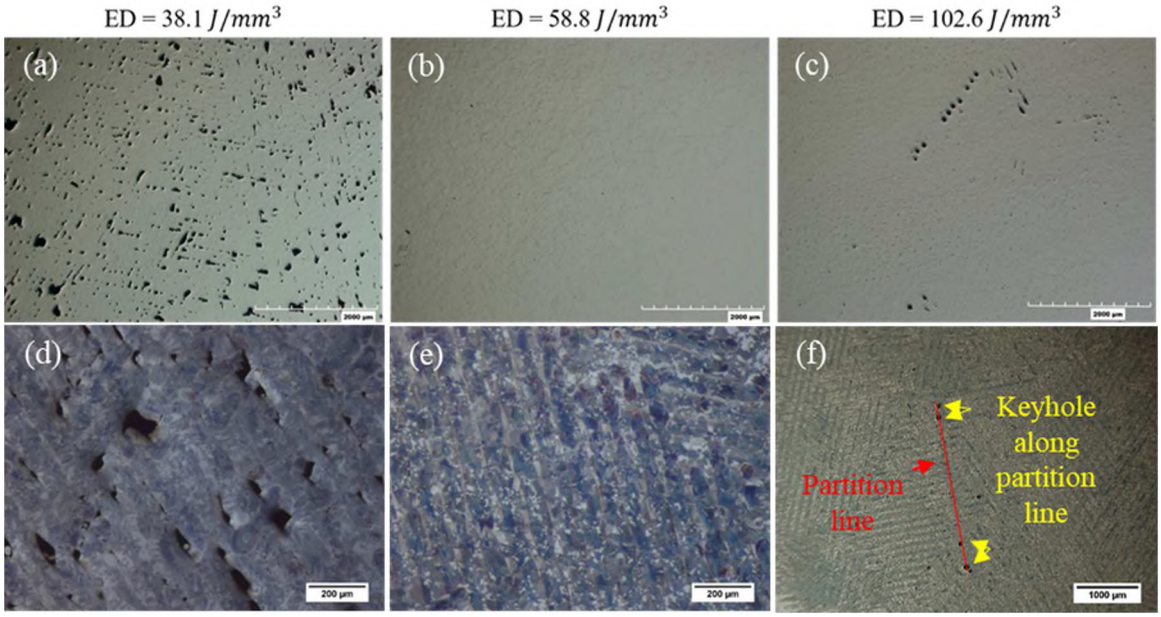

Figure 7. As polished x-y (in layer) cross-section OM images of (a) ED #15, (b) ED #8 and (c) ED #1. Microstructure images of x-y (in layer) cross-section under different magnifications: (d) ED #15, (e) ED #8 and (f) ED #1 showing the spherical pores built up along the partition line.

To evaluate the validity of the above-mentioned reasoning, the above pictured polished sections were etched to reveal the location of porosity relative to the microstructural features of the LBPF material. The electrolytic etching method used in this investigation was observed to reveal features such as in-layer track boundaries, the cellular dendritic microstructures, and emphasize porosity. As seen from Figure 7 (d), the location of the pores and streaks of pores in material made using ED #15 was observed to be along the track boundaries in x-y sections indicating the insufficient overlaps between adjacent

laser scans. Similar to Figure 7 (b), image (Figure 7 (e)) after etching of ED #8 revealed the scan patterns in a layer without revealing any apparent porosity. Figure 7 (f) depicts the localized gas porosity which was induced along the partition line at ED #1. This was possibly due to the vaporization of previously solidified material along the partition line.

3.3. HARDNESS

To assess the influence of ED variation on hardness, both microhardness and hardness testing were performed on the above imaged polished cross-sections and shown in Figure 8. In the case of the microhardness values, no obvious trends were observed. However, significant differences were observed among a few of the energy densities. Even if statistically significant, the scale of the difference, from a practical standpoint was deemed negligible. The hardness values, on the other hand, were observed to be lower than the microhardness values. The hardness of the specimen with the lowest ED was observed to be the lowest and most variant. This observation can be attributed to the presence of porosity. Generally speaking, the median hardness values tracked well with the median density values. Once the density was above 99%, the hardness values were observed to be similar.

3.4. TENSILE PROPERTIES

Similar to the effect of ED/density on hardness, the variation in tensile performance was also studied. The 0.2% offset yield strength, ultimate tensile strength, and maximum elongation were measured and analyzed. The anisotropy in the mechanical properties of additively manufactured material has been extensively reported [29–32]. To assess this

phenomenon in LPBF AISI 304L, tensile specimens were cut in two orientations. One, along the build direction and two, perpendicular to the build direction. This would imply that the gage length is vertical i.e. along the build direction in the first case and horizontal i.e. perpendicular to the build direction in the second case. The YS and UTS measurements are plotted in Figure 9 (top and middle, respectively).

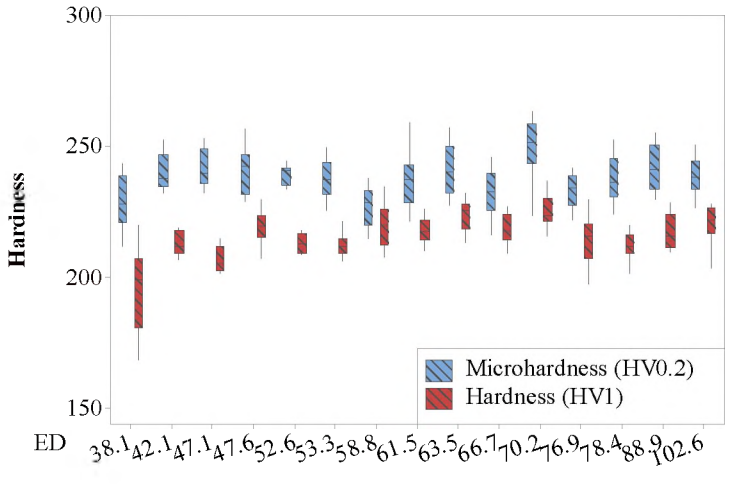

Figure 8. Micro-hardness and Vickers hardness data in the plane.

Statistically significant differences in yield strength were observed with varying energy density for both cut orientations. However, no discernable trends were observed. At the lowest energy density of 38.1 J/mm^3 the yield strength was measured to be 453.2 ± 12.5 and 426.8 ± 9.3 MPa in the horizontal and vertical orientation, respectively. The rest of the median values of yield strength varied from 480.6 to 513.1 MPa for horizontal orientation and from 447.8 to 485.7 MPa for vertical orientation. Overall, the yield strength measurements from vertical specimens were lower than the yield strength measurements from horizontal specimens. This was true of all the specimens of all the considered energy

densities. The difference between the vertical and horizontal yield strength was also found to be statistically significant.

Larger differences in UTS were observed in two cut orientations. In the lower energy density region (<52.6 J/mm^3), an obvious initial increase in UTS could be seen with ED, then UTS stabilized with ED. The overall trend of UTS with ED was similar to bulk density. Hence, it is believed that the higher amount of lack of fusion porosity gave rise to the lower UTS. A 2.53%±0.16% porosity could produce a UTS of 617.3 ± 13.6 MPa in the horizontal orientation and 536.0 ± 18.5 MPa in the vertical orientation. With bulk density, more than 99%, the highest median UTS of built specimens can achieve to 711.4 MPa in horizontal and 653.6 MPa in the vertical orientation. It was also worth mentioning that specimens cut in horizontal orientation behaved an almost 100 MPa higher in strength than that in the vertical orientation. The weaker bonding, hence lower strength, between layers than along layers could contribute to this phenomenon; however further investigation needs to be done to confirm.

Elongation measurements from specimens cut along the vertical and horizontal orientations are plotted in Figure 9 (bottom plot). Generally speaking, elongation performance increased with increasing density. This was true for specimens cut in both orientations. The material with the largest amount of porosity produced a median elongation of 30% and 55% for horizontal and vertical orientations respectively. For the material with porosity above 1%, the median elongation of vertical specimens was lower than that of the horizontal specimens. For material under the 1% porosity limit, the median vertical elongation was higher than that of the horizontal orientation. This flip in elongation performance can be attributed to the presence of excessive lack of fusion porosity between

layers in the material. The fracture surfaces of the broken tensile specimens printed with ED #8 in two orientations were examined. The presence of the lack of fusion porosity is apparent from Figure 10 (a) in vertical and (c) in horizontal. Similar irregular shaped pores/voids with trapped powder were noticed on examined specimens. Zoom-in plots in Figure (b) for vertical and (d) for horizontal exposed the fine dimple features demonstrating the ductile fracture mode for both orientations.

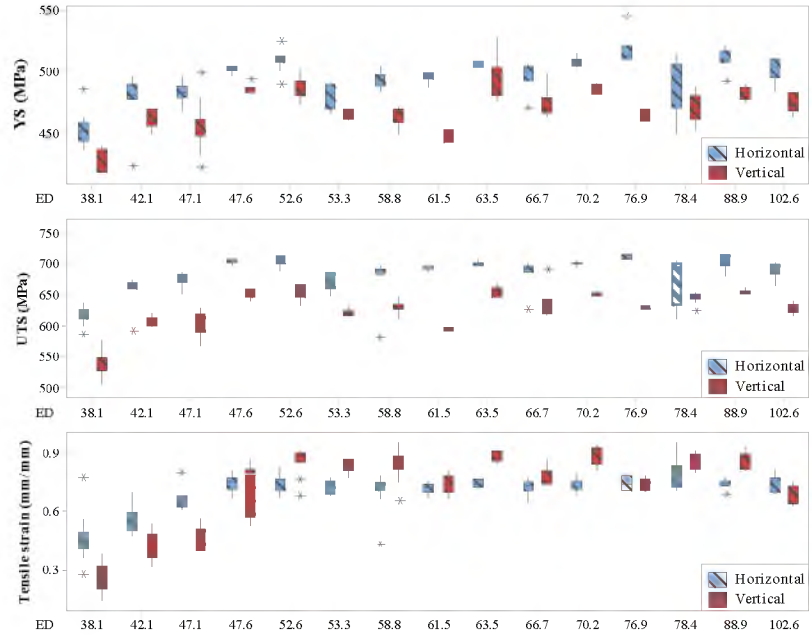

Figure 9. The tensile strengths of the test specimens cut in two orientations.

The anisotropy in performance is theorized to be an effect of the total amount of porosity sampled and the difference in loading direction relative to the location and orientation of said porosity. Besides, according to the Hall-Petch effect, strength improvement is proportional to an inverse square root of the mean grain size for polycrystalline alloys. Tensile anisotropies of 304 steel were little dependent on the texture

or crystal structures, but the columnar microstructures played significant roles. During tensile testing, the specimens built in horizontal direction had major axes perpendicular to the loading direction while parallel to the loading direction for vertical specimens. Hence, the effective grain sizes in the horizontal direction were smaller than those in vertical orientation due to more grain boundaries in the horizontal direction [36,37]. On the other hand, during the propagation stage of tensile testing, the cracks preferably propagate along the near-vertical columnar grain boundaries [38], hence, specimens built in the horizontal direction were easier to propagate in comparison with those fabricated in vertical, which gave rise to lower elongations [36].

3.5. IMPACT TOUGHNESS

The impact toughness of Charpy specimens built in vertical orientation vs. energy density for each parameter set is charted as a box plot, shown in Figure 11. For benchmarking purposes, specimens of commercially sourced cold-rolled and annealed AISI 304 were tested for impact toughness performance. The median of impact toughness of this wrought material was measured to be 210 J and highlighted with a red dash line in Figure 11 [30]. The general trend in the variation of impact toughness appeared to be a parabola. The highest median toughness was observed for the energy density of 77 J/mm^3 (parameter set #6 hereon called tou-opt). For energy density higher than 77J/mm^3, the impact toughness was observed to drop. This drop of toughness was observed to occur without any compromise of bulk density. Parameter set #6, tou-opt, achieved a median toughness value higher than that of wrought material. A 3% volumetric porosity reduced the toughness by more than 80%. Also, at a low porosity area (<1%), the difference in

impact toughness still could be seen. Keyhole porosity was suspected to be the reason for the drop at higher ED.

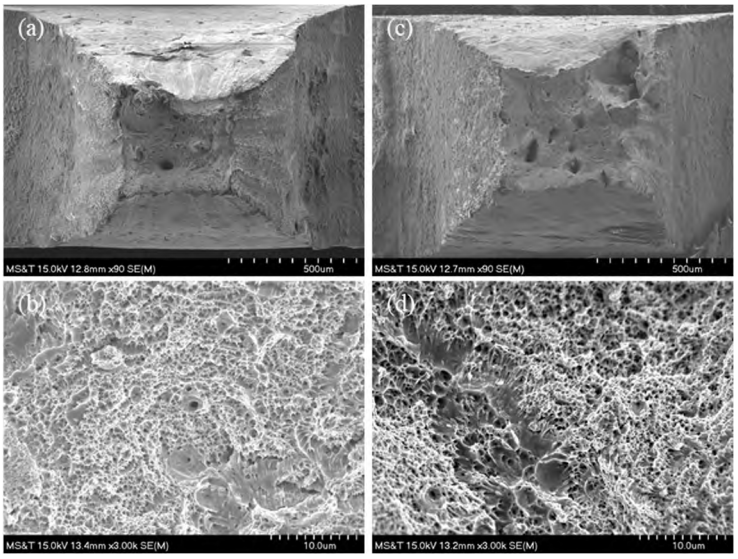

Figure 10. Fractography of broken miniature tensile specimens cut in (a) vertical with (b) zoom-in image and (c) horizontal orientation with (d) zoom-in image built with the parameter set #8.

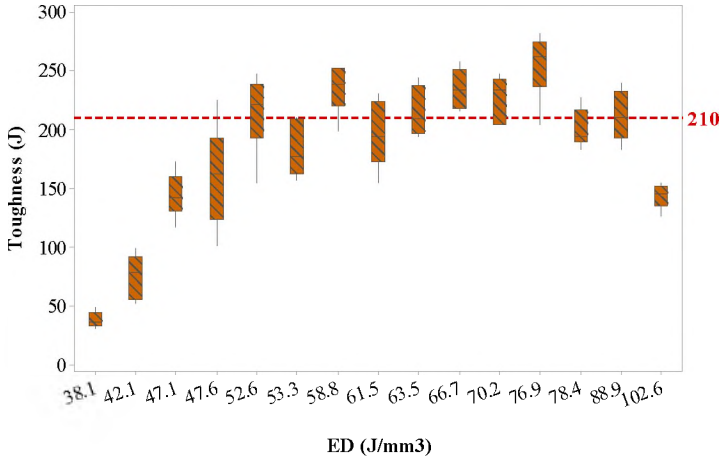

Figure 11. The impact toughness vs. ED. The red dash line indicates the median toughness of rolled and annealed 304L stainless steel tested in previous work [23].

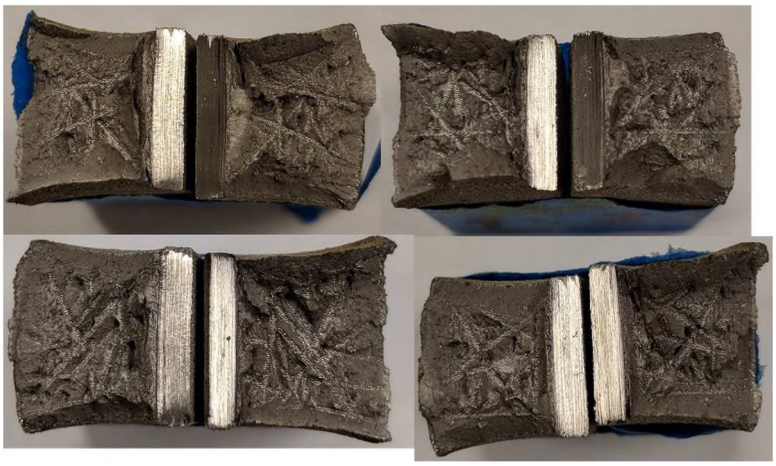

Figure 12. The fracture surface of broken Charpy specimens built with the highest ED #1.

To demonstrate the claim, the macro images were captured for the fracture surface of broken Charpy specimens fabricated with the different ED, which is shown in Figure 12. It was interesting to note that, the unique line marks on the fracture surface were suspected to be a series of keyhole pores produced due to vaporization from remelting along the partition line at different build layers. These line marks were also consistent with the cross-section image built with the highest ED in Figure 7. The keyhole pores seemed to be produced along a straight line. Those line marks could be one of the potential reasons for the decrease in impact toughness at higher ED.

Furthermore, the fracture surfaces were examined with SEM and categorized with different hatch spacing and scan speed in Figure 13. At a higher ED region with lower hatch spacing and scan speed (highlighted with a blue border), step-like features were dominant on the fracture surfaces possibly induced by the 90° direction changes from one layer boundary to the adjunct layer boundary. Interestingly, line marks composed of keyhole porosity along the partition line (highlighted with red arrow) were also observed

on the fracture surface of the highest ED with the lowest hatch spacing and scan speed, which was believed to be the potential reason for the decrease of impact toughness at high ED. In the middle ED region, the trough/pit-like features with rounded natures were indicative of ductile fracture mode. Excessive groups of parallel line features were captured on the fracture surfaces in the low ED region. The width of the parallel line feature at each ED was measured to be similar to the corresponding hatch spacing, hence, those line features could be produced by the poor bonding and overlap between the adjacent scan lines in layers.

3.6. MATERIAL CHARACTERIZATION OF TOU-OPT PARAMETER

The specimens built with the tou-opt parameter set possessed the best median toughness value among all 15 parameter sets in the vertical orientation. A previous study [35] suggested a significant difference in impact toughness due to the anisotropy issue for printed 304L stainless steel built with a nominal parameter. It was also crucial to see how the anisotropy issue affects the newly developed process parameter optimized for toughness. The densities of the fabricated specimens with the tou-opt parameter built in three orientations are plotted in Figure 14. No significant difference in density was revealed with different build orientations.

The tested impact toughness for specimens built in three orientations is shown in Figure 15. In our previous work [35], specimens built with the nominal parameter exhibited the lower toughness in the vertical orientation than that in the horizontal and inclined orientation. However, for the tou-opt parameter set, the horizontal specimens possessed the lowest median of toughness while the vertical specimens showed the highest

median of toughness, also accompanied by the largest variability. It was believed that the difference in ED altered the shape and depth of the melt pool, hence, the bonding strength between layers and the ease of crack propagation along the interlayer track boundary varied with ED. However, inconsistencies still existed in the vertical Charpy specimens, which induced the highest variation of the toughness.

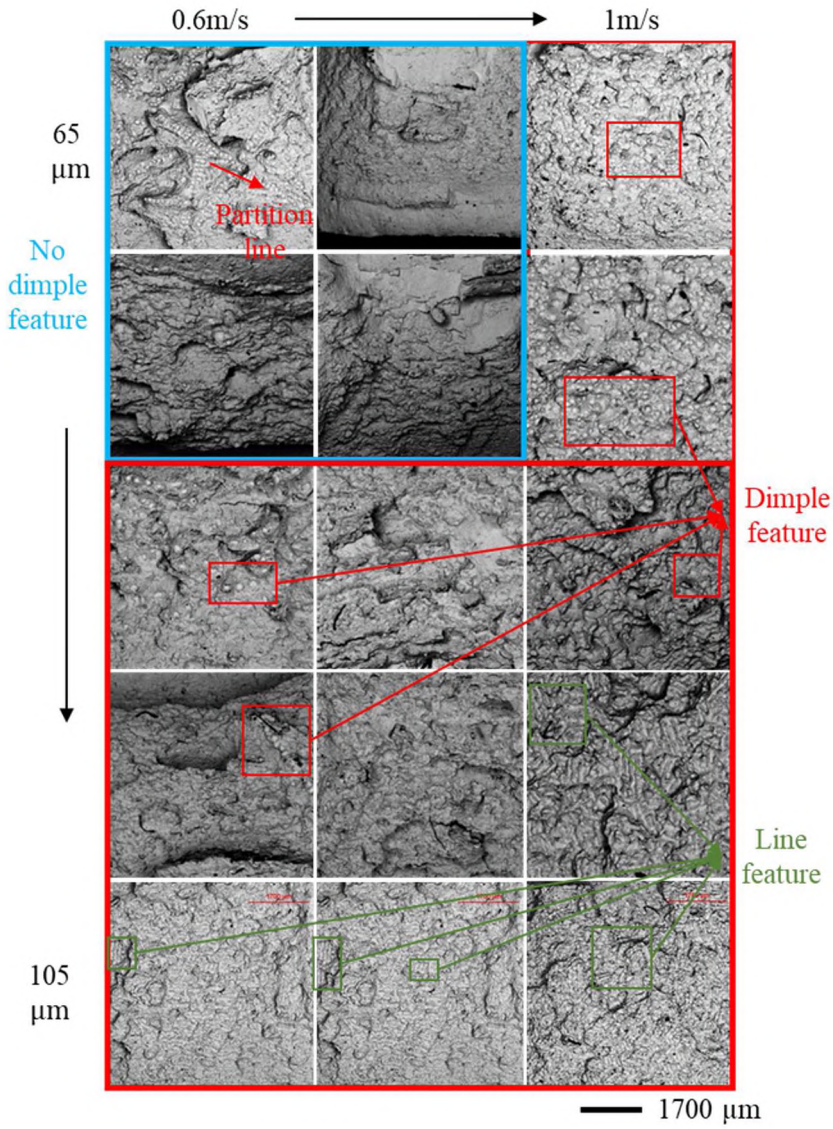

Figure 13. The fracture surfaces of the broken Charpy specimens built with different ED representing by 5 levels of hatch spacing and 3 levels of scan speed.

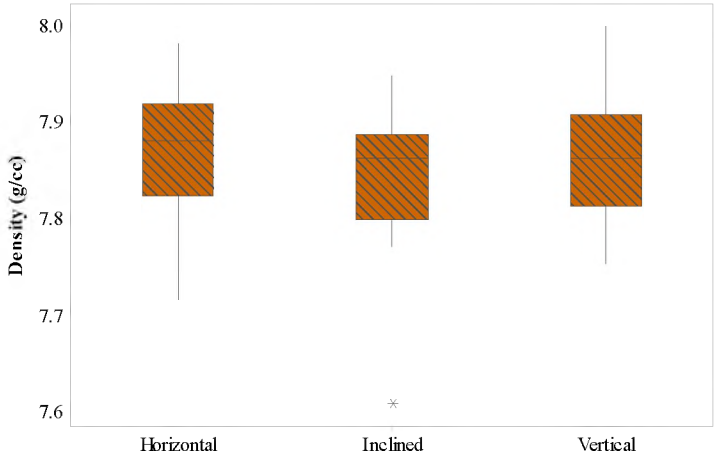

Figure 14. The density for specimens built with tou-opt parameter in three build orientations.

Figure 16 (a), (b), and (c) illustrate the fracture surfaces of broken Charpy specimens printed in three build orientations. Generally speaking, the crack was propagated with a smoothly varying path. The step-like features were possibly induced by the 90° direction changes from one melt pool boundary to adjacent melt pool boundary. Much less smooth trough/pit-like features seen in Figure 13 could be observed in three build orientations, which was dissimilar to those seen on the fracture surface of specimens built with nominal parameters [35] where the rounded natures of the trough/pit-like features indicated the likelihood that the crack was propagated along the melt pool boundaries. High magnification images were shown in Figure 16 (e) to (f) for horizontal, inclined, and vertical, respectively. The appearance of surface texture and small dimple features indicated a ductile mode of failure. Indications of scattered porosity and the presence of inclusions were also observed. These inclusions with one of them highlighted with a yellow arrow in Figure 16 (e) were observed to be rich in Mn and Cr.

4. CONCLUSION

In this study, the aim is to build up a process-properties map by quantifying the bounds of mechanical properties of LPBF stainless steel 304L fabricated with a range of energy densities. 15 EDs were procured by varying five levels of the hatch spacing and three levels of the scan speed. The specimens fabricated with 15 EDs were characterized by their densifications, microstructures, hardness, tensile properties, and impact toughness. Anisotropies in mechanical performances were investigated with different build orientations.

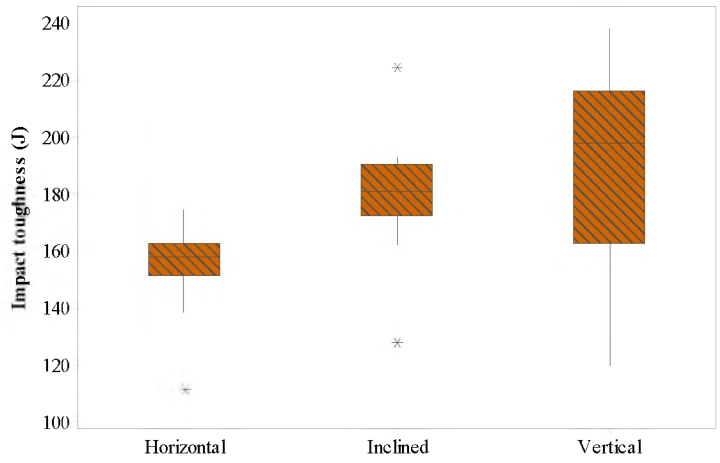

Figure 15. The impact toughness for specimens built with tou-opt parameter in three orientations.

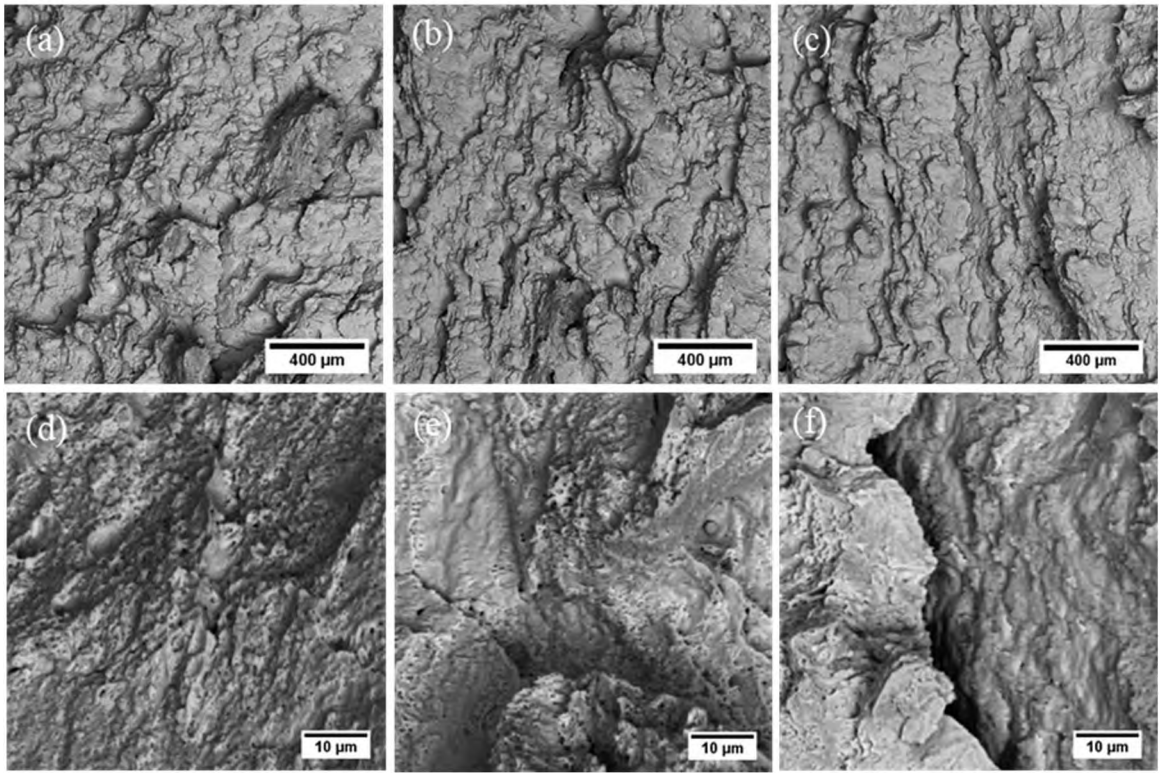

Figure 16. The fracture surface of broken Charpy specimens built with tou-opt parameter in (a) horizontal (b) inclined and (c) vertical orientation; (d) zoomed-in image of (a); (e) zoomed-in image of (b) with an inclusion highlighted with a yellow arrow; and (f) zoomed-in image of (c).

Density testing indicated the densities of fabricated specimens were greater than 99% when EDs were not less great than 47.6 J/mm^3. At lower ED, Microstructure examination under OM revealed the presence of the irregular shaped pores and streaks of such pores. This porosity was attributed to on account of lack of fusion and insufficient overlap between successive layers and tracks layers at low ED (high scan speed and hatch spacing). At the middle ranges of the intermediate ED, porosity was rarely found. However, linear formations of spherical gas porosity were identified at the highest ED. These formations were with the localization along the partition line and were suspected to be

originating due to the exceeding energy-input vaporization induced by the remelting along the partition line.

Hardness testing demonstrated the hardness values were to be comparable when the density achieved density was more than 99% (equivalent to ED no less than 47.6J/mm^3). No discernable trends of yield strength were observed with ED while the trend of UTS with ED was similar to that of density with ED. For the low ED range, lack of fusion was the main reason leading to the decrease in UTS. The highest UTS among all ED was 711.4 MPa and 653.6 MPa in the horizontal and vertical orientation, respectively.

For specimens with porosity less than 1%, elongations in vertical orientation were larger than those in the horizontal orientation. For specimens with porosity greater than 1%, the elongation in the vertical direction was lower than the horizontal. This behavior was attributed to the presence of a lack of fusion porosity. Fractography pointed out a ductile failure mode among all the tensile tested specimens.

The trend curve of median impact toughness vs. ED seemed to be a parabola with the highest median impact toughness shown at ED of 77 J/mm^3 (tou-opt). This value was higher than the toughness of wrought material. The development of keyhole porosity along the partition line was suspected to be the reason for the drop of toughness at higher EDs.

Anisotropy in impact toughness was explored with the optimized process parameter set, tou-opt. Specimens printed with tou-opt in three build orientations revealed an insignificant difference in density. Horizontal specimens exhibited the lowest median of toughness while the vertical specimens showed the highest median of toughness accompanied with the largest variation. The change in ED seemed to improve the anisotropy by reducing the variation in median impact toughness.

ACKNOWLEDGEMENTS

This work was funded by Honeywell Federal Manufacturing & Technologies under Contract No. DE-NA0002839 with the U.S. Department of Energy.

REFERENCES

1. Bhavar, V.; Forge, B.; Kattire, P. A review on powder bed fusion technology of metal additive manufacturing Business development of Additive Manufacturing View project additive manufacturing View project. 2014.

2. Kruth, J.P.; Leu, M.C.; Nakagawa, T. Progress in additive manufacturing and rapid prototyping. CIRP Ann. - Manuf. Technol. 1998, 47, 525–540.

3. Li, R.; Liu, J.; Shi, Y.; Wang, L.; Jiang, W. Balling behavior of stainless steel and nickel powder during selective laser melting process. Int. J. Adv. Manuf. Technol. 2012, 59, 1025–1035.

4. Mukherjee, T.; DebRoy, T. Mitigation of lack of fusion defects in powder bed fusion additive manufacturing. J. Manuf. Process. 2018, 36, 442–449.

5. Mercelis, P.; Kruth, J. Residual stresses in selective laser sintering and selective laser melting. Rapid Prototyp. J. 2006, 12, 254–265.

6. Kimura, T.; Nakamoto, T. Microstructures and mechanical properties of A356 (AlSi7Mg0.3) aluminum alloy fabricated by selective laser melting. Mater. Des. 2016, 89, 1294–1301.

7. Gong, H.; Rafi, K.; Gu, H.; Starr, T.; Stucker, B. Analysis of defect generation in Ti-6Al-4V parts made using powder bed fusion additive manufacturing processes. Addit. Manuf. 2014, 1, 87–98.

8. Gu, H.; Gong, H.; Pal, D.; Rafi, K.; Starr, T.; Stucker, B. Influences of energy density on porosity and microstructure of selective laser melted 17- 4PH stainless steel. Solid Free. Fabr. 2013, 474–479.

9. Wang, C.; Tan, X.; Liu, E.; Tor, S.B. Process parameter optimization and mechanical properties for additively manufactured stainless steel 316L parts by selective electron beam melting. Mater. Des. 2018, 147, 157–166.

10. Sun, Z.; Tan, X.; Tor, S.B.; Yeong, W.Y. Selective laser melting of stainless steel 316L with low porosity and high build rates. Mater. Des. 2016, 104, 197–204.

11. Yusuf, S.; Chen, Y.; Boardman, R.; Yang, S.; Gao, N. Investigation on Porosity and Microhardness of 316L Stainless Steel Fabricated by Selective Laser Melting. Metals (Basel). 2017, 7, 64.

12. Hu, Z.; Zhu, H.; Zhang, H.; Zeng, X. Experimental investigation on selective laser melting of 17-4PH stainless steel. Opt. Laser Technol. 2017, 87, 17–25.

13. Wang, P.; Tan, X.; He, C.; Nai, M.L.S.; Huang, R.; Tor, S.B.; Wei, J. Scanning optical microscopy for porosity quantification of additively manufactured components. Addit. Manuf. 2018, 21, 350–358.

14. Yasa, E.; Kruth, J.P. Microstructural investigation of selective laser melting 316L stainless steel parts exposed to laser re-melting. Procedia Eng. 2011, 19, 389–395.

15. Zikmund, T.; Šalplachta, J.; Zatočilová, A.; Břínek, A.; Pantělejev, L.; Štěpánek, R.; Koutný, D.; Paloušek, D.; Kaiser, J. Computed tomography based procedure for reproducible porosity measurement of additive manufactured samples. NDT E Int. 2019, 103, 111–118.

16. Rashid, R.; Masood, S.H.; Ruan, D.; Palanisamy, S.; Rahman Rashid, R.A.; Brandt, M. Effect of scan strategy on density and metallurgical properties of 17-4PH parts printed by Selective Laser Melting (SLM). J. Mater. Process. Technol. 2017, 249, 502–511.

17. Ziółkowski, G.; Chlebus, E.; Szymczyk, P.; Kurzac, J. Application of X-ray CT method for discontinuity and porosity detection in 316L stainless steel parts produced with SLM technology. Arch. Civ. Mech. Eng. 2014, 14, 608–614.

18. Zhang, B.; Dembinski, L.; Coddet, C. The study of the laser parameters and environment variables effect on mechanical properties of high compact parts elaborated by selective laser melting 316L powder. Mater. Sci. Eng. A 2013, 584, 21–31.

19. Yasa, E.; Kruth, J.P. Microstructural investigation of selective laser melting 316L stainless steel parts exposed to laser re-melting. Procedia Eng. 2011, 19, 389–395.

20. Deng, P.; Peng, Q.; Han, E.H.; Ke, W.; Sun, C.; Jiao, Z. Effect of irradiation on corrosion of 304 nuclear grade stainless steel in simulated PWR primary water. Corros. Sci. 2017, 127, 91–100.

21. Mukhopadhyay, C.K.; Jayakumar, T.; Raj, B.; Ray, K.K. The influence of notch on the acoustic emission generated during tensile testing of nuclear grade AISI type 304 stainless steel. Mater. Sci. Eng. A 2000, 276, 83–90.

22. Chiang, M.F.; Hsu, H.H.; Young, M.C.; Huang, J.Y. Mechanical degradation of cold-worked 304 stainless steel in salt spray environments. J. Nucl. Mater. 2012, 422, 58–68.

23. Chiang, M.F.; Young, M.C.; Huang, J.Y. Effects of hydrogen water chemistry on corrosion fatigue behavior of cold-worked 304L stainless steel in simulated BWR coolant environments. J. Nucl. Mater. 2011, 411, 83–89.

24. Nguyen, Q.B.; Zhu, Z.; Ng, F.L.; Chua, B.W.; Nai, S.M.L.; Wei, J. High mechanical strengths and ductility of stainless steel 304L fabricated using selective laser melting. J. Mater. Sci. Technol. 2018, 35, 388–394.

25. Grubb, J.F.; Ludlum, A.; Fritz, J.D.; Stainless, T.M.R. Corrosion of Wrought Stainless Steels. Corros. Mater. 2018, 13, 54–77.

26. Tucho, W.M.; Lysne, V.H.; Austbø, H.; Sjolyst-Kverneland, A.; Hansen, V. Investigation of effects of process parameters on microstructure and hardness of SLM manufactured SS316L. J. Alloys Compd. 2018, 740, 910–925.

27. Cherry, J.A.; Davies, H.M.; Mehmood, S.; Lavery, N.P.; Brown, S.G.R.; Sienz, J. Investigation into the effect of process parameters on microstructural and physical properties of 316L stainless steel parts by selective laser melting. Int. J. Adv. Manuf. Technol. 2014, 76, 869–879.

28. Guan, K.; Wang, Z.; Gao, M.; Li, X.; Zeng, X. Effects of processing parameters on tensile properties of selective laser melted 304 stainless steel. Mater. Des. 2013, 50, 581–586.

29. Liverani, E.; Toschi, S.; Ceschini, L.; Fortunato, A. Effect of selective laser melting (SLM) process parameters on microstructure and mechanical properties of 316L austenitic stainless steel. J. Mater. Process. Technol. 2017, 249, 255–263.

30. Suryawanshi, J.; Prashanth, K.G.; Ramamurty, U. Mechanical behavior of selective laser melted 316L stainless steel. Mater. Sci. Eng. A 2017, 696, 113–121.

31. Casati, R.; Lemke, J.; Vedani, M. Microstructure and Fracture Behavior of 316L Austenitic Stainless Steel Produced by Selective Laser Melting. J. Mater. Sci. Technol. 2016, 32, 738–744.

32. Kurzynowski, T.; Gruber, K.; Stopyra, W.; Kuźnicka, B.; Chlebus, E. Correlation between process parameters, microstructure and properties of 316 L stainless steel processed by selective laser melting. Mater. Sci. Eng. A 2018, 718, 64–73.

33. Brown, B.; Liou, F. Characterization of 304L Stainless Steel Parameter Sets on the Selective Laser Melting Platform. 2014, Paper 7322.

34. S. Karnati, I. Axelsen, F. F. Liou, J.W.N. Investigation of Tensile Properties of Bulk and Slm Fabricated 304L Stainless Steel Using Various Gage Length Specimens. Solid Free. Fabr. 2016, 13.

35. Karnati, S.; Khiabhani, A.; Flood, A.; Liou, F.; Newkirk, J. Anisotropy in impact toughness of powder bed fused AISI 304L stainless steel. Mater. Des. Process. Commun. 2019, e59.

36. Yu, H.; Yang, J.; Yin, J.; Wang, Z.; Zeng, X. Comparison on mechanical anisotropies of selective laser melted Ti-6Al-4V alloy and 304 stainless steel. Mater. Sci. Eng. A 2017, 695, 92–100.

37. Wang, Z.; Palmer, T.A.; Beese, A.M. Effect of processing parameters on microstructure and tensile properties of austenitic stainless steel 304L made by directed energy deposition additive manufacturing. Acta Mater. 2016, 110, 226–235.

38. Carroll, B.E.; Palmer, T.A.; Beese, A.M. Anisotropic tensile behavior of Ti-6Al-4V components fabricated with directed energy deposition additive manufacturing. Acta Mater. 2015, 87, 309–320.

SECTION

2. CONCLUSIONS AND RECOMMENDATIONS

2.1. CONCLUSIONS

The current study aimed to extend the existing knowledge of AISI 304L fabricated by Laser PBF by establishing the process-property map. The impact of different process parameters on mechanical performance and anisotropy was investigated, which supports the future study on this material. The main conclusions were extracted and listed as following.

- By varying the scan speed and hatch spacing, ED ranging from 38.1 J/mm^3 to 102.6 J/mm^3 were established which were adopted to print parts possessing density ranging from ~97% to >99%. A minimum of 47.6 J/mm^3 was revealed to be necessary to obtain the relative density > 99%.
- No perceptible differences in hardness could be detected with varying ED.
- The variation of yield strength was not discernable with ED while UTS vs. ED showed a similar trend to that of density vs. ED. At higher porosity, the vertical elongation was lower than that in the horizontal orientation. On the contrary, elongation in vertical orientation was greater than horizontal orientation where porosity < 1%.
- At $77 J/mm^3$, specimens revealed the highest median value of impact toughness, which was extraordinary compared to wrought material. Keyhole-type porosity accumulated along the partition lines due to

excessive remelting was suspected to be the reason for the decrease in toughness at higher ED. The anisotropy in impact performance was altered with two input energies.

2.2. RECOMMENDATIONS

In this study, tensile properties, hardness, and impact toughness were investigated with the variation of the energy density, and tou-opt process parameter was identified as the optimal parameter which maximized the impact toughness without compromise of tensile properties and modified the anisotropy in impact performance. However, fatigue properties draw more attentions nowadays, hence, it is recommended that the fatigue strength and possible anisotropy in fatigue could be tested out for the parts printed with a new parameter.

BIBLIOGRAPHY

1. Bhavar, V.; Forge, B.; Kattire, P. A review on powder bed fusion technology of metal additive manufacturing Business development of Additive Manufacturing View project additive manufacturing View project. **2014**.

2. Ziółkowski, G.; Chlebus, E.; Szymczyk, P.; Kurzac, J. Application of X-ray CT method for discontinuity and porosity detection in 316L stainless steel parts produced with SLM technology. *Arch. Civ. Mech. Eng.* **2014**, *14*, 608–614.

3. Wang, C.; Tan, X.; Liu, E.; Tor, S.B. Process parameter optimization and mechanical properties for additively manufactured stainless steel 316L parts by selective electron beam melting. *Mater. Des.* **2018**, *147*, 157–166.

4. Zhang, B.; Dembinski, L.; Coddet, C. The study of the laser parameters and environment variables effect on mechanical properties of high compact parts elaborated by selective laser melting 316L powder. *Mater. Sci. Eng. A* **2013**, *584*, 21–31.

5. Sun, Z.; Tan, X.; Tor, S.B.; Yeong, W.Y. Selective laser melting of stainless steel 316L with low porosity and high build rates. *Mater. Des.* **2016**, *104*, 197–204.

6. Yasa, E.; Kruth, J.P. Microstructural investigation of selective laser melting 316L stainless steel parts exposed to laser re-melting. *Procedia Eng.* **2011**, *19*, 389–395.

7. Yusuf, S.; Chen, Y.; Boardman, R.; Yang, S.; Gao, N. Investigation on Porosity and Microhardness of 316L Stainless Steel Fabricated by Selective Laser Melting. *Metals (Basel).* **2017**, *7*, 64.

8. Zikmund, T.; Šalplachta, J.; Zatočilová, A.; Břínek, A.; Pantělejev, L.; Štěpánek, R.; Koutný, D.; Paloušek, D.; Kaiser, J. Computed tomography based procedure for reproducible porosity measurement of additive manufactured samples. *NDT E Int.* **2019**, *103*, 111–118.

9. Gu, H.; Gong, H.; Pal, D.; Rafi, K.; Starr, T.; Stucker, B. Influences of energy density on porosity and microstructure of selective laser melted 17- 4PH stainless steel. *Solid Free. Fabr.* **2013**, 474–479.

10. Hu, Z.; Zhu, H.; Zhang, H.; Zeng, X. Experimental investigation on selective laser melting of 17-4PH stainless steel. *Opt. Laser Technol.* **2017**, *87*, 17–25.

11. Wang, P.; Tan, X.; He, C.; Nai, M.L.S.; Huang, R.; Tor, S.B.; Wei, J. Scanning optical microscopy for porosity quantification of additively manufactured components. *Addit. Manuf.* **2018**, *21*, 350–358.

12. Tucho, W.M.; Lysne, V.H.; Austbø, H.; Sjolyst-Kverneland, A.; Hansen, V. Investigation of effects of process parameters on microstructure and hardness of SLM manufactured SS316L. *J. Alloys Compd.* **2018**, *740*, 910–925.

13. Cherry, J.A.; Davies, H.M.; Mehmood, S.; Lavery, N.P.; Brown, S.G.R.; Sienz, J. Investigation into the effect of process parameters on microstructural and physical properties of 316L stainless steel parts by selective laser melting. *Int. J. Adv. Manuf. Technol.* **2014**, *76*, 869–879.

14. Wang, D.; Song, C.; Yang, Y.; Bai, Y. Investigation of crystal growth mechanism during selective laser melting and mechanical property characterization of 316L stainless steel parts. *Mater. Des.* **2016**, *100*, 291–299.

15. Guan, K.; Wang, Z.; Gao, M.; Li, X.; Zeng, X. Effects of processing parameters on tensile properties of selective laser melted 304 stainless steel. *Mater. Des.* **2013**, *50*, 581–586.

16. Shifeng, W.; Shuai, L.; Qingsong, W.; Yan, C.; Sheng, Z.; Yusheng, S. Effect of molten pool boundaries on the mechanical properties of selective laser melting parts. *J. Mater. Process. Technol.* **2014**, *214*, 2660–2667.

17. Liverani, E.; Toschi, S.; Ceschini, L.; Fortunato, A. Effect of selective laser melting (SLM) process parameters on microstructure and mechanical properties of 316L austenitic stainless steel. *J. Mater. Process. Technol.* **2017**, *249*, 255–263.

18. Casati, R.; Lemke, J.; Vedani, M. Microstructure and Fracture Behavior of 316L Austenitic Stainless Steel Produced by Selective Laser Melting. *J. Mater. Sci. Technol.* **2016**, *32*, 738–744.

19. Suryawanshi, J.; Prashanth, K.G.; Ramamurty, U. Mechanical behavior of selective laser melted 316L stainless steel. *Mater. Sci. Eng. A* **2017**, *696*, 113–121.

20. Nguyen, Q.B.; Zhu, Z.; Ng, F.L.; Chua, B.W.; Nai, S.M.L.; Wei, J. High mechanical strengths and ductility of stainless steel 304L fabricated using selective laser melting. *J. Mater. Sci. Technol.* **2018**, *35*, 388–394.

21. Ahmadi, A.; Mirzaeifar, R.; Moghaddam, N.S.; Turabi, A.S.; Karaca, H.E.; Elahinia, M. Effect of manufacturing parameters on mechanical properties of 316L stainless steel parts fabricated by selective laser melting: A computational framework. *Mater. Des.* **2016**, *112*, 328–338.

22. S. Karnati, I. Axelsen, F. F. Liou, J.W.N. Investigation of Tensile Properties of Bulk and Slm Fabricated 304L Stainless Steel Using Various Gage Length Specimens. *Solid Free. Fabr.* **2016**, 13.

23. Karnati, S.; Khiabhani, A.; Flood, A.; Liou, F.; Newkirk, J. Anisotropy in impact toughness of powder bed fused AISI 304L stainless steel. *Mater. Des. Process. Commun.* **2019**, e59.

VITA

Tan Pan received her Bachelor of Science degree in Petroleum Engineering from Missouri University of Science and Technology (Missouri S&T) and Northeast Petroleum University in May, 2017. She started pursuing her master's degree as a graduate research assistant under the supervision of Dr. Frank Liou in Manufacturing Engineering at Missouri S&T in August 2017. She received her Master of Science degree in Manufacturing Engineering from Missouri S&T in August 2020.